

## Research Article

# An Unconventional Approach for Analyzing the Mechanical Properties of Natural Fiber Composite Using Convolutional Neural Network

Govindaraj Ramkumar <sup>1</sup>, Satyajeet Sahoo <sup>2</sup>, G. Anitha <sup>1</sup>, S. Ramesh <sup>3</sup>, P. Nirmala <sup>1</sup>,  
M. Tamilselvi <sup>4</sup>, Ram Subbiah <sup>5</sup> and S. Rajkumar <sup>6</sup>

<sup>1</sup>Department of Electronics and Communication Engineering, Saveetha School of Engineering, SIMATS, Chennai 602105, Tamil Nadu, India

<sup>2</sup>Department of Electronics and Communication Engineering, Vignan's Foundation for Science, Technology and Research (Deemed to be University), Vadlamudi, Guntur, Andhra Pradesh 522213, India

<sup>3</sup>Department of Electronics and Communication Engineering, Sri Shakthi Institute of Engineering and Technology, Coimbatore-641062, Tamil Nadu, India

<sup>4</sup>Department of Mechatronics Engineering, T.S. Srinivasan Centre For Polytechnic College and Advanced Training, Chennai, Tamil Nadu, India

<sup>5</sup>Department of Mechanical Engineering, Gokaraju Rangaraju Institute of Engineering and Technology, Nizampet, Hyderabad, India

<sup>6</sup>Department of Mechanical Engineering, Faculty of Manufacturing, Institute of Technology, Hawassa University, Awasa, Ethiopia

Correspondence should be addressed to Govindaraj Ramkumar; [pgrvlsi@gmail.com](mailto:pgrvlsi@gmail.com) and S. Rajkumar; [rajkumar@hu.edu.et](mailto:rajkumar@hu.edu.et)

Received 19 July 2021; Revised 4 August 2021; Accepted 16 August 2021; Published 24 August 2021

Academic Editor: Ravichandran M

Copyright © 2021 Govindaraj Ramkumar et al. This is an open access article distributed under the Creative Commons Attribution License, which permits unrestricted use, distribution, and reproduction in any medium, provided the original work is properly cited.

Over the past few years, natural fiber composites have been a strategy of rapid growth. The computational methods have become a significant tool for many researchers to design and analyze the mechanical properties of these composites. The mechanical properties such as rigidity, effects, bending, and tensile testing are carried out on natural fiber composites. The natural fiber composites were modeled by using some of the computation techniques. The developed convolutional neural network (CNN) is used to accurately predict the mechanical properties of these composites. The ground-truth information is used for the training process attained from the finite element analyses below the plane stress statement. After completion of the training process, the developed design is authorized using the invisible data through the training. The optimum microstructural model is identified by a developed model embedded with a genetic algorithm (GA) optimizer. The optimizer converges to conformations with highly enhanced properties. The GA optimizer is used to improve the mechanical properties to have the soft elements in the area adjacent to the tip of the crack.

## 1. Introduction

In the current situation, industries were mostly focused on the sustainable idea of manufacture to minimize the non-renewable resources procedure and adopt the process of ecofriendly materials by waste reuse or recycling. To prepare composite materials, extensive work is done by the

researcher in several areas of the world [1]. Polymer and natural fiber composites have been selected as ideal materials due to necessary characteristics including reusability, recyclability, long-term constancy, and widespread accessibility at a reasonable cost. When compared to synthetic fibers, natural fibers have inferior qualities such as significant water absorption, weak bonding, low durability, and

low mechanical and thermal properties on industrial applications. The optimization and modeling computational engineers employ some approaches to deal with the mechanical difficulties that arise in science and engineering research [2].

Researchers in the field of materials engineering are investigating these computational methods that may be used to model and optimize the many properties of composite materials reinforced with natural fibers. Due to various environmental concerns, the goal is possibly replacing synthetic fibers and environmental considerations [3]. Fiber treatment, nanofilter addition, and hybridization are a few technologies that have been developed to overcome these restrictions. The use of these technologies to manufacture natural fiber composite (NFC) materials has broadened their range of applications such as household, structural, sporting, automobile, aerospace, and other manufacturing applications in recent decades [4].

The process of analyzing the natural fiber's quality and the composites that arise is complicated, which makes it challenging to establish generic methods for modeling and optimizing composite qualities [5]. The use of current computational approaches for studying the characteristics of NFCs has proven to be helpful in the modeling and optimization of composite materials. The shielding process of mechanical properties on natural fiber composites is done by using the electromagnetic interference (EMI). The shielding of EMI efficiency, microstructure, flexibility, tensile, and inner bonding strength of the composites are examined. The EMI excellent shielding performance and mechanical properties use the composite materials in the EMI protection fields. Researchers and producers can easily determine the best mix of constituent materials to balance the strength and cost of the resultant materials by using computational or mathematical models. The analysis of the relationship between the input and output parameters in materials processing is part of composite material modeling.

A deep neural network is inspired by the biological neural network architectures processing the learning data obtained from the user. This network usually has input, hidden, and output layers [6]. The DNN is used to succeed in finite element analysis while solving the optimization problem of graded functionality plates. A DNN for forecasting foamed concrete compressive strength models was trained on a huge number of photos, and then their learning ability was transferred to pavement fracture identification using digitized pavement surface images.

A convolutional neuronal network (CNN) model makes it possible to quantitatively predict the mechanical properties of the compound through maximum fraction space volume [7]. CNNs are a type of DNN, and they were chosen because of their performance in image recognition tasks. In the following sections, taking into account all the volume fractions considerably expands the sample space. Also, from a practical perspective, having a model that forecasts composite performance of actual standards instead of classes list derived from an organization model is more helpful [8]. In addition, using an optimization approach depends on GA with the model CNN created for optimizing mechanical

properties in terms of stiff and soft material volume fraction and spatial distribution in the microstructure.

The remaining part of this paper is as follows. Section 2 describes the previous effort that was done by the scholars in this domain with the various experimental tasks; Section 3 offers the materials and methods, Section 4 represents the evaluation and performance of the result and discussion; and Section 5 represents the work achieved in conclusion.

## 2. Literature Survey

Munde and Ingle (2015) evaluates interest in minimum environmental and inexpensive pollution. This research is focused on biocomposite mechanical properties using the models of available theory and investigational authentication of mechanical properties. Parallel and series, modified Halpin-Tsai, Hirsch model, and Halpin-Tsai are the theoretical models used for mechanical tensile properties evaluation. To prepare the sample specimen by using the compression molding machine, the characterization of the mechanics is performed ASTM D638-01 through the universal test machine. The results compared the assumed modulus of tensile and strength of tensile with the characteristics of mechanical properties [9]. De Araujo Alves Lima et al. (2020) analyzed alkalization influence. By combining the behavior of alkalization and silanization on the adhesion interfacial and intralaminar hybrid composite's mechanical properties, the single tensile fiber examined fragmentation and also performed the tests of the short beam. Finally, the analysis of SEM is used to research the surface chemical influence treatment used on the natural fibers morphology, to improve the fiber tensile strength by the research of chemical treatment and alkaline treatment on fibers such as ramie, curaua, and jute. After the fusion treatment, there are better results from the presented sisal fibers. The best treatment of being superficial for individual types of composites is the alkaline treatment for fibers obtaining better results for the untreated samples [10].

Sridharan and Muthukrishnan (2013) evaluate, during the machining and production, whether biocomposites require less energy. The quality of fiber is enhanced by using different chemical treatments. The process of mercerization is improving the composite mechanical properties significantly. This research compares the machinability of reinforced composite jute fiber organized using processed and untreated alkaline fiber. The value of the hole is depending on a comparison of the delamination factor achieved through digital image processing techniques. The experiments are based on the factorial design conducted at the various levels of feed rate and velocity. The ANOVA (analysis of variance) is used to research the chemical treatment influence on delamination. To find the condition of optimum drilling, the Grey Relational Analysis (GRA) is employed [11]. Sultana et al. (2020) estimate the various soft approaches for computing such as Response Surface Methodology (RSM), Artificial Neural Network (ANN), and Support Vector Regression (SVR) for nonlinear empirical development models to expect the mechanical properties of Jute Fiber Reinforced Concrete

Composites (JFRCC). The water-cement relationship (W/C), the capacity of jute fibers, and the length are the most dependent properties. The data for JFRCC properties are matrix-design-based and these data are used to plan, compare, and estimate the models. Thus, the act of the SVR model is better than RSM and ANN models with different performance and parameters measuring to predict both tensile and compressive strengths [12].

Wang, Wu, and Wang (2010) evaluate the fiber aspect ratio effect on steel fiber reinforced concrete (SFRC) mechanical characteristics. This analysis exposes the aspect ratio of the best parameter for strength in every batch. The steel fibers addition can relatively increase the effect of ductility. The erosion-based algorithm is used for numerically simulated steel projects on two SFRC targets such as perforation and crater. Due to the postyield injury, the behavior of softening model has tabulated the effective plastic strain and effective stress. These results show that the hydrodynamic model described the SFRC responses under effect loading. In addition, the higher appearance ratio of the fiber engages high energy causing reduced craters in the SFRC goal and less remaining rate of the projectile [13]. Table 1 shows the various mechanical properties of natural fiber composites.

### 3. Materials and Method

The composite material of natural fibers was modeled using certain computation methods in this research. The materials include mechanical properties such as jute, sugarcane, ramie, pineapple, and banana fibers. The various parameters are observed from the mechanical characteristics of natural fiber composites. The natural hybrid composites are fabricated through the process of vacuum-assisted rein transfer molding (VARTM). The composites presented better electromagnetic interference (EMI) shielding performance with better mechanical properties. The properties are inherited from the aluminum sheets and natural fiber composites. Currently, the natural fiber composites have mechanical properties of inferiority when compared to the parts of the synthetic counter [21]. The two or more fibers that are dissimilar are get mixed in a common matrix to create a composite panel in the hybrid composite. The hybridization is achieved by merging the different lengths and dissimilar diameters for small fibers. This method aims to evaluate the mechanical properties and shielding performance of natural fiber composites. Next, the content of the nanofiller is used to overcome the limitations of the composite material that is reinforced in natural fibers to enhance dimensional stability. Figure 1 shows the manufacturing of man-made fibers from raw materials.

**3.1. Modeling of Mechanical Properties of Natural Fiber Composites.** Modeling the mechanical properties of natural fibers composite materials is considered a complex process due to different parameters including the matrix type, used fiber, overall composition, the process of manufacturing, the process of fabrication, and planned applications. The

composites offered electromagnetic interference (EMI) for shielding performance with better mechanical properties. Researchers have been able to build these improved modeling approaches with better precision due to recent advances in processing capacity. The goal is to review some computational modeling methodologies that have been employed in the study of fiber-reinforced composite materials.

**3.2. Rule of Hybrid Mixture (RoHM).** The Rule of Hybrid Mixture (RoHM) model considers that the structure is made up of more than one fiber embedded in one matrix material as a hybrid composite [22]. Applying the isostrain state condition to a reinforced hybrid composite with the two fibers yields equation (1), where  $\varepsilon_{co}$ ,  $\varepsilon_{m1}$ ,  $\varepsilon_{m2}$  denote the total material strain, initially fiber strain, and next fiber strain. By assuming no interplay between each type of fiber, the equation of RoHM is modeled to compute the hybrid composite modulus as shown in equation (2). Then  $L_{co}$ ,  $U_{r1}$ , and  $U_{r2}$  represent the hybrid composite elasticity and qualified volume fraction of hybrid composite for initial and next fibers.

$$\varepsilon_{co} = \varepsilon_{m1} + \varepsilon_{m2}, \quad (1)$$

$$L_{co} = L_{r1}U_{r1} + L_{r2}U_{r2}, \quad (2)$$

Equations (1) and (2) are under the following conditions:  $U_{r1} + U_{r2} = 1$ ,  $U_{r1} = U_{m1}/U_f$ ,  $U_{r2} = U_{m2}/U_f$  and  $U_f = U_{m1} + U_{m2}$ , where  $U_f$  is the complete reinforcement fraction volume upon the  $(U_{m1} + U_{m2})$ , which is basically used as the volume fraction of reinforcement for the elasticity computation ( $L_{r1}$  and  $L_{r2}$ ) of the both exclusive composites. Tensile strength and density fraction of banana module/sisal fiber in variable ratios using experiments and applying RoHM are considered a predictor tool. The comparison between the exact experimental results and the RoHM tensile strength results is shown in Figures 2 and 3 which allows for concluding the methods.

**3.3. Halpin-Tsai Model.** The model of Halpin-Tsai is employed to expect the composite material elastic modulus using fiber elasticity, materials of the matrix, and geometry as input parameters [23]. The empirical approach is considered, the field approach of self-consistency from the basic model. The model offers that the modulus of tensile and strength of tensile composite material is given in (3) and (4), where  $S_a$ ,  $S_d$ ,  $I_a$ ,  $I_d$  represent the composite elastic moduli, matrix elastic moduli, matrix tensile strength, and composite tensile strength, respectively.  $U_m$  represents the volumetric fraction of fibers in composites. The parameter value of  $F = J - 1$  and  $J = 1 + 2s/t$ , where the diameters of fiber and length are denoted as  $t$  and  $s$ , respectively. The parameter  $\gamma$  is given by equation (5) and (6). The parameter of  $F$  measures the geometry of fiber, distribution of fiber, and loading of fiber condition.  $I_m$  and  $S_m$  represent the moduli of elastic and tensile strength of the fiber, respectively. The

TABLE 1: List of various mechanical properties of natural fiber composites.

| Reference | Fiber      | Matrix | Strength of tensile (MPa) | Stiffness (GPa) | Strength of flexural (MPa) | Modulus flexural |
|-----------|------------|--------|---------------------------|-----------------|----------------------------|------------------|
| [14]      | Sisal      | Epoxy  | 212                       | 6               | 320                        | 27               |
| [15]      | Banana     | Epoxy  | 46                        | 8               | —                          | —                |
| [16]      | Flax       | Up     | 147                       | 14              | 198                        | 17               |
| [16]      | Hemp       | Epoxy  | 165                       | 17              | 180                        | 9                |
| [16]      | Coir       | Epoxy  | 225                       | 6               | —                          | —                |
| [17]      | Jute       | PP     | 74                        | 11              | 112                        | 12               |
| [18]      | Kenaf      | PLA    | 223                       | 23              | 259                        | 22               |
| [16]      | Oil palm   | PP     | 53                        | 2               | 80                         | 3                |
| [19]      | Sisal/Hemp | PLA    | 60.23                     | 6.1             | 79.76                      | 6.04             |
| [20]      | Jute/Sisal | Epoxy  | 74.78                     | 6.76            | —                          | —                |

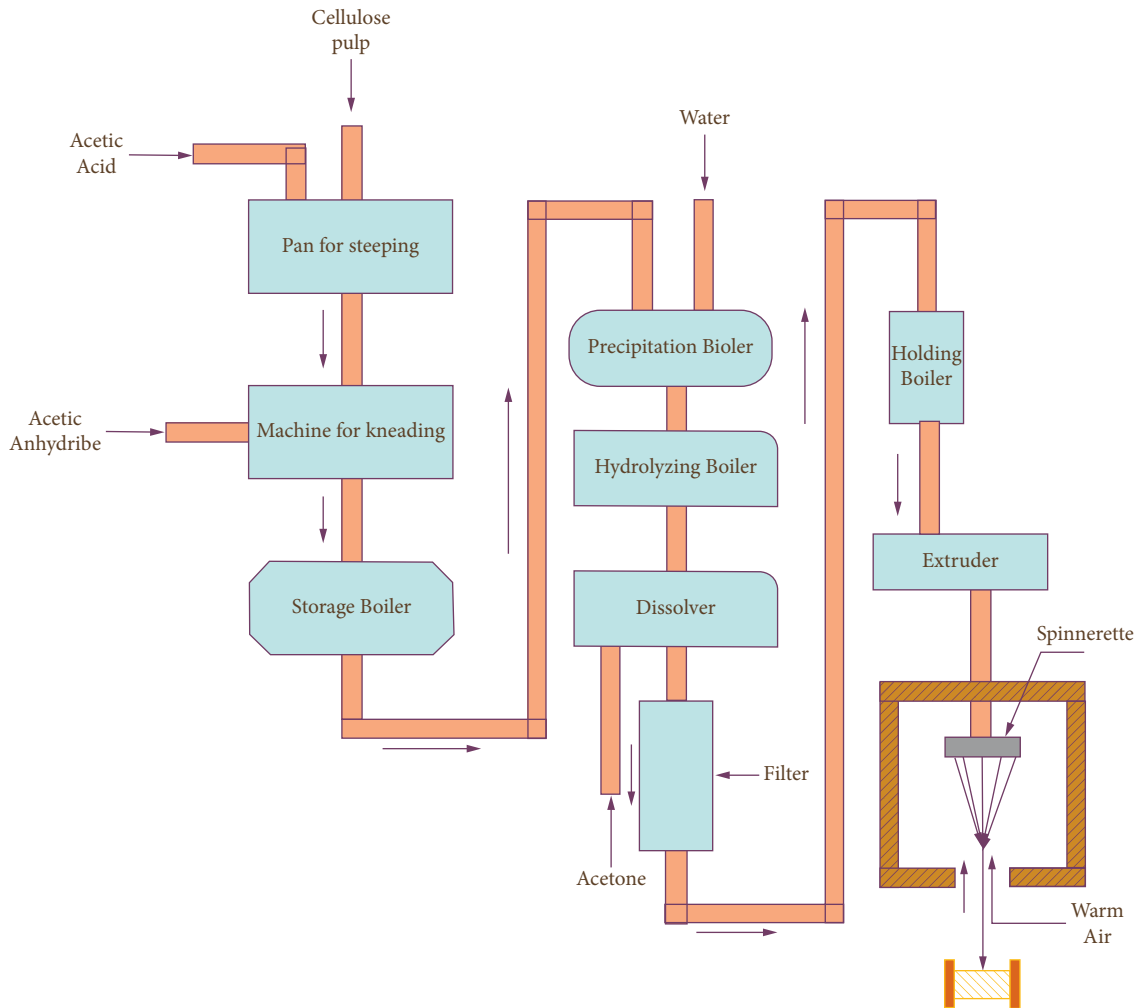


FIGURE 1: Manufacturing of man-made fibers.

Halpin–Tsai model’s essential equations are used to explain the issues analytically to determine the natural occurrence of the structure’s fluctuation. The results obtained after using the optimization revealed a higher frequency attained by the hybrid nanocomposites compared with nonhybrid composites.

$$S_a = S_d \left[ \frac{1 + F_\gamma U_m}{1 + \gamma U_m} \right], \quad (3)$$

$$I_a = I_d \left[ \frac{1 + F_\gamma U_m}{1 + \gamma U_m} \right], \quad (4)$$

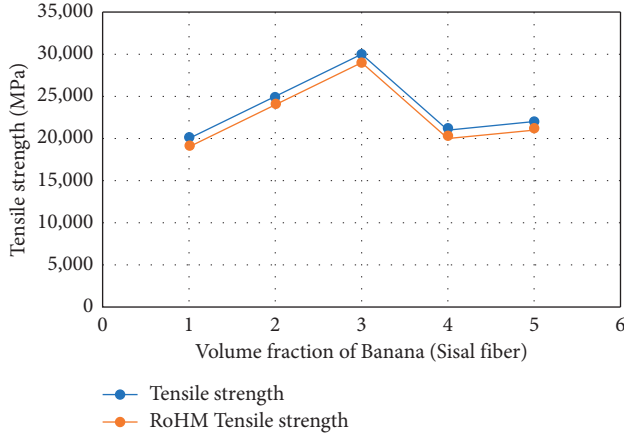


FIGURE 2: Experimental and RoHM tensile strength of banana/sisal fiber composites results.

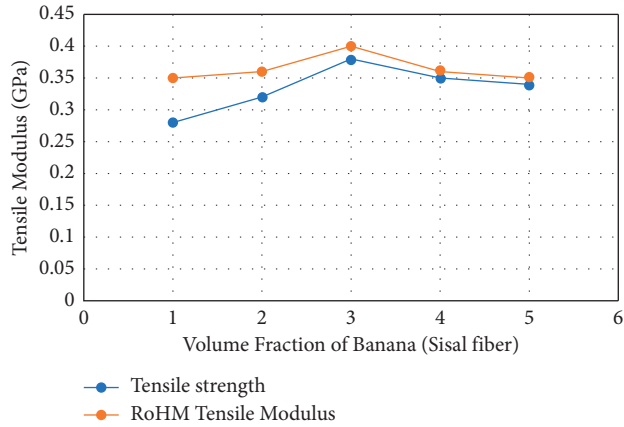


FIGURE 3: Experimental and RoHM tensile modulus of banana/sisal fiber composites results.

$$\gamma = \frac{S_m/S_d - 1}{S_m/S_d + F}, \quad (5)$$

$$\gamma = \frac{I_m/I_d - 1}{I_m/I_d + F}. \quad (6)$$

**3.4. Model of Hirsch.** The model is concerned with the sequence stacking and fiber orientation in a matrix material [24]. A diagram of the Hirsch model is given in Figure 4 which shows the parallel and series mixture models. Thus, equation (5) shows the composite characteristics, where  $I_a$ ,  $I_d$ , and  $I_m$  represent the composite strength of tensile, matrix material strength of tensile, and fibers tensile strength.  $U_d$  denotes the matrix volume fraction and  $U_m$  denotes the fraction of fiber volume.

$$I_a = z(I_d U_d + I_m U_m) + (1 - z) \frac{I_m I_d}{I_d U_m + I_m U_d}. \quad (7)$$

$z$  in the equation indicates a variable amount which gives the load transfer between the fiber and the array. The Hirsch model is used to determine the best characteristics of tensile

hybrid composite, which reveals that the mechanical performance is modifiable between the values 0.37 and 0.55.

**3.5. Electromagnetic Interference for Shielding Process.** Figure 5 shows that A2, A3, A2H11, and A3H12 are investigated using the micro-A1 sheets. The EMI shielding occurs through the radiation reflection. The EMI shielding is the most popular method by using metal sheets and coating. The metal sheets are regularly used, but some suffer from drawback on the bad mechanical properties and resistance corrosion. The metal sheets are converted into the natural fiber composites. The EMI shielding process results from using metal sheets and thus having better mechanical properties given by the natural fiber composites. The metal sheets are protected to avoid the electrochemical corrosion by natural fiber composites. The microstructures of EMI shielding performance and the mechanical properties of the composites are examined.

**3.6. Convolutional Neural Network Model.** The convolutional neural network model is designed to predict the rigidity, toughness, and strength of two material fibers, one rigid and brittle and the other soft and ductile [25]. The CNN technique model frequently needs important data to provide the exact prediction of fibers. During the training process, it examines new data that is invisible to the model following the formation of the CNN model. The CNN model is based on the data of an FEA (Finite Element Analysis).

The FEA is performed to estimate the interest assets. The replication of the finite elements is motionless when the von Mises ( $\epsilon_{vs}$ ) deformation at the crack point reaches the corresponding fracture deformation. Then, the von Mises strain is explained as

$$\epsilon_{vs} = \frac{2}{3} \left( \frac{3}{2} (\epsilon_{11}^2 + \epsilon_{22}^2 + \epsilon_{33}^2) + \frac{3}{4} \epsilon_{12}^2 \right)^{1/2},$$

$$\epsilon_{11} = \frac{\sigma_{11}}{V} - \frac{u\sigma_{22}}{V}, \quad \epsilon_{22} = \frac{\sigma_{22}}{V} - \frac{u\sigma_{11}}{V}, \quad \epsilon_{12} = \frac{1+u}{V} \sigma_{12}. \quad (8)$$

Young's modulus value for stiff fiber is  $V = 1$  GPa, and the value of soft fiber material is  $V = 0.1$  GPa. The Poisson relationship for both flexible and rigid fiber materials is  $u = 1/3$ . The break deformation of brittle and rigid fiber materials is 10%, although the break deformation of soft and ductile fiber materials is expected to be 100%. Consider three active qualities of fibers: modulus, strength, and toughness. In FEA, four-node elements were used when the individual section has one point of four quadratures and the individual part has one degree of the two freedoms [26]. The cracked fibers have two dissimilar sizes assumed as  $8 \times 8$  and  $16 \times 16$  size systems as examples for the input.

Finite Element Analysis (FEA) is conducted to create data critical to this research. Consider both grid sizes  $8 \times 8$  and  $16 \times 16$  as illustrated in Figure 6. The FE approach is used to study a large amount of alternative complex

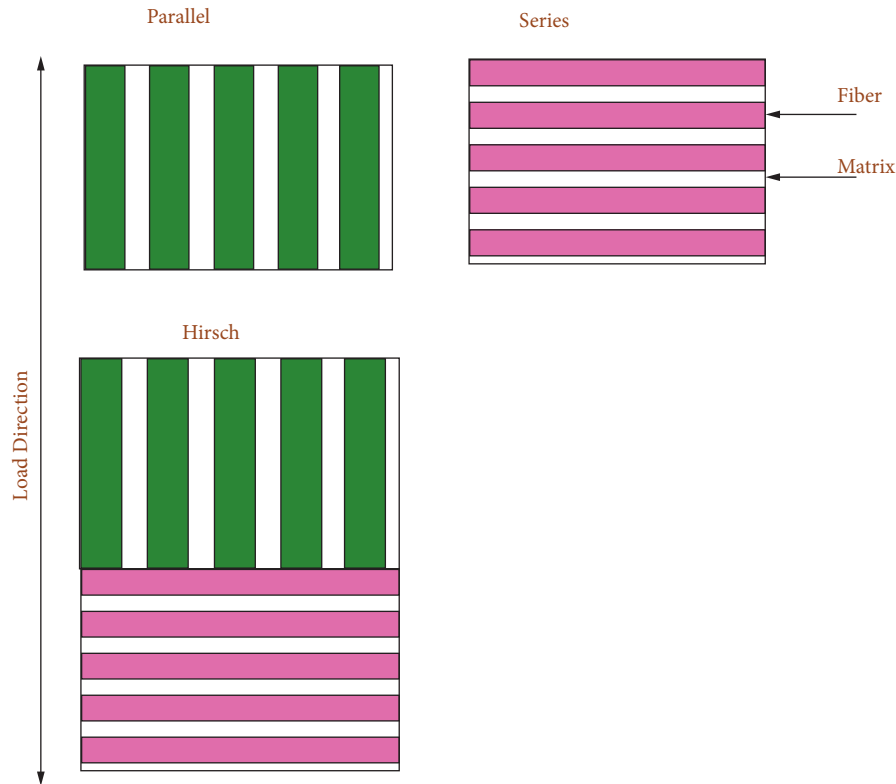


FIGURE 4: Hirsch model diagram.

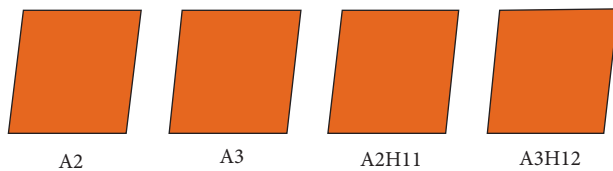


FIGURE 5: The fabrication composites diagram.

arrangements corresponding to the two grid sizes, and the resultant characteristics within each structure are recorded. The microstructure, containing information on volume fractions and phase spatial distributions, is called configuration. Some preprocessing processes are required after obtaining data from the FEA to make the information for feeding into the CNN model [27]. A matrix is a representation of data in its most basic form from the acquired FEA. The training instances are represented in the rows of that matrix, while the binary distribution of the materials is represented in the columns as 0 for stiffness and 1 for softness. Every learning algorithm has a labeled vector that contains the three material properties: strength, toughness, and strength. Each function is translated into an image by specifying the spatial model for every component to be supplied into the CNN model, whose convolutions could be conducted to develop the CNN model.

The key strategy of a CNN is that the input data are or may be viewed as a picture. As a result, the set of variables is reduced greatly, resulting in speedier processing. In

Figure 7, the convolutional layer, pooling layers, fully connected layers, and beginning purposes are the layers that make up a typical CNN. A filter is connected to the input image by an activation function in the convolutional layer, which maintains the interconnections between pixel values. A pooling layer combines the input layer as max-pooling that yields the best accuracy division from every session. Layered and simulation functions in fully linked DNN systems are comparable to those in simple DNN structures [28]. The next layer, such as stall layers, which are the regulation strategies to minimize model overflow, may also be added to CNN. Two CNN architectures were developed in each dimension grid with six fused layers, one exclusion layer, and one fully connected layer in the respective architecture. Each composite layer consists of a 2D convolution layer, a 2D batch stabilization layer, and a corrected linear part activation (ReLU) function. The convolutional layers kernel scopes are varied between the two architectures.

**3.7. Evaluation of CNN Model.** The mean square error (MSE) cost purpose is used during the formation phase to reduce the residual error among the output data model and the ground-truth data. The average absolute percentage error (MAPE) is used to calculate the model precision. Equations (9) and (10) are used to calculate the mean square and the mean absolute percent error to measure the difference between the actual and projected values.

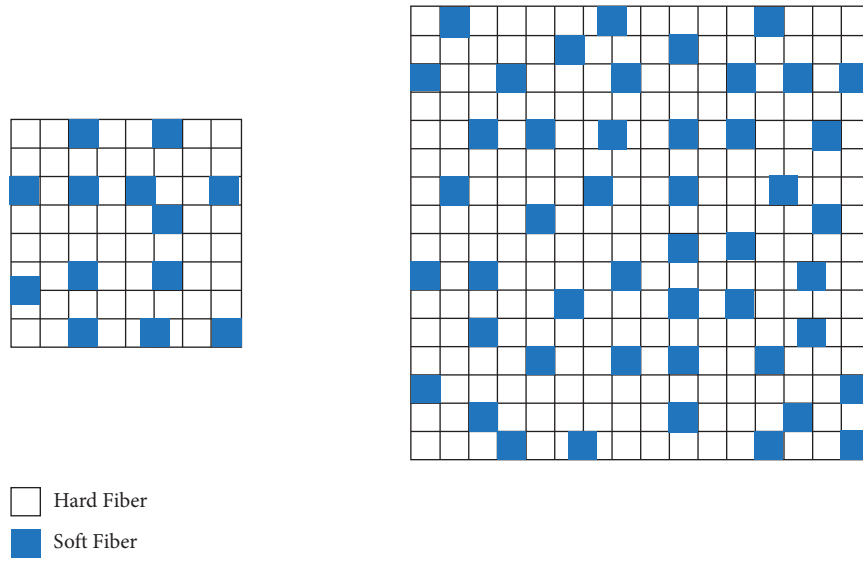


FIGURE 6: 8 × 8 grid and 16 × 16 grid.

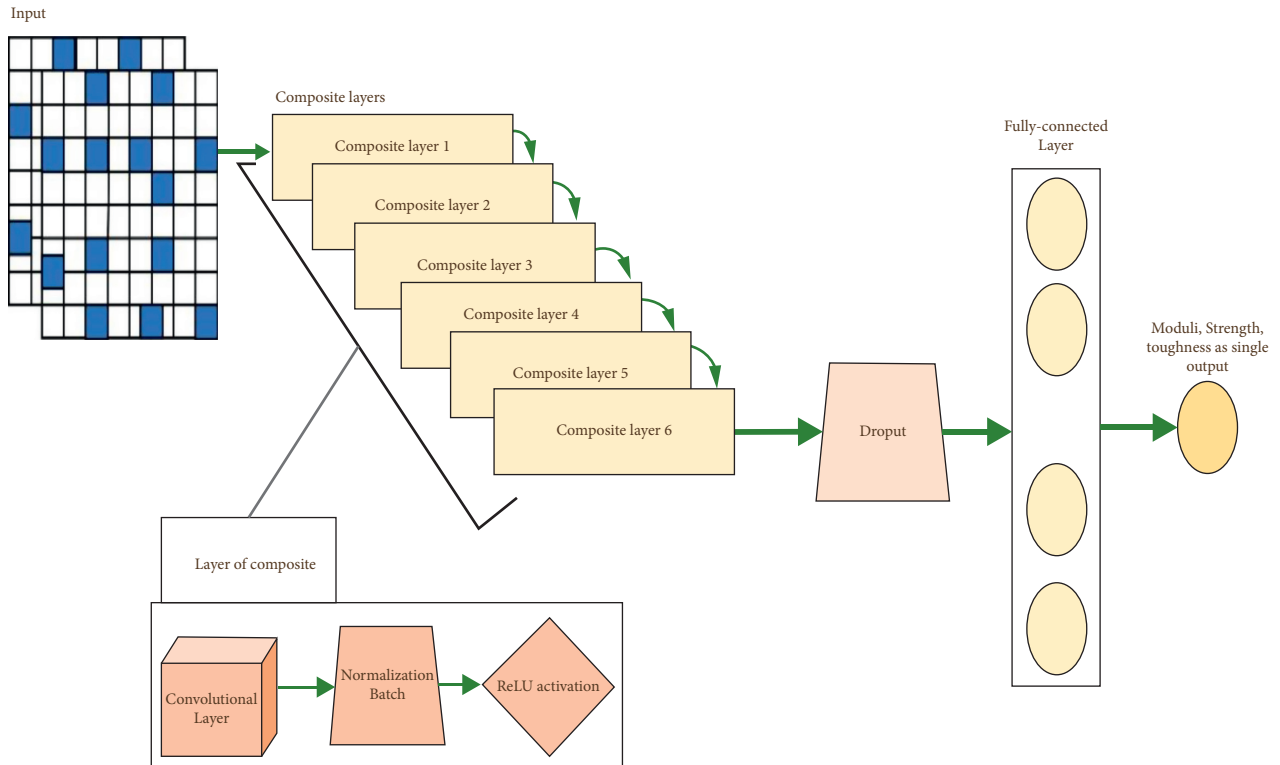


FIGURE 7: Schematic diagram of CNN model.

$$MSE = \frac{1}{a} \sum_{n=1}^a (k_n - \hat{k}_n)^2, \quad (9)$$

where  $\hat{k}_n$  is the prediction found based on the model and  $k_n$  is the real value.

$$MAPE = \frac{1}{a} \sum_{n=1}^a \left| \frac{k_n - \hat{k}_n}{k_n} \right|, \quad (10)$$

3.8. *Genetic Algorithm for Optimization.* The various bio-inspired operators such as crossover, mutation, and selection are frequently used in GA optimizers to obtain the optimal

solutions. The GA optimizer selects random individuals from the last generation as parents generating offspring for subsequent generations through each optimization process [29]. The roulette wheel mechanism is utilized as the selection operator, with greater fitness values yielding a larger selection probability. The frequency of the optimal solution in an optimization system is called fitness.

A genetic algorithm is a type of computer-based research and optimization algorithm that depends on natural genetics and natural selection mechanics. Other conventional optimization methods are less likely to provide optimal global coverage than the GA. The reason for this is that GA is based on probabilistic criteria and research based on a population of the points in inherited space. Traditional optimization strategies are usually based on deterministic research which uses the idea of the gradient to localize local optima. Each genetic operation cycle is referred to as a developing process. The fitness of every member of the population was assessed in each generation and subsequent generations were formed using the chromosomes of the current population. This entails the mixing and recombination of genes from both parents to produce offspring in the following generation. Reproduction, mutation, and crossover are all parts of the evolution process. The optimization problem as is follows:

$$a_i^{(U)} \leq a_i \leq a_i^{(V)}, a_i = p_1, p_2. \quad (11)$$

$a_i$  are decoded with this linear mapping rule:

$$a_i = a_i^{(U)} + \frac{(a_i^{(V)} - a_i^{(U)})}{2^{ui-1}} \text{ is decoded value } (t_i), \quad (12)$$

where  $a_i = p_1, p_2$ ;  $(U)$  = minimum limitation;  $(V)$  = maximum limitation;  $ui$  = binary bit count; and  $t_i$  = equivalent of decimal values.

A chromosome relates to some microstructures that store the material around it to form a specific microstructure element. A uniform distribution is used to choose the first generation at random. The suitability of a microstructure is determined independently of the break of the generational chromosomes. The technique for using the genetic algorithm is shown in Figure 8.

## 4. Results and Discussion

The efficiency of the linear model is associated with the CNN model. To develop a linear model quantitatively based on the composite properties, the equation in the linear model is given as follows:

$$M = XC + Y, \quad (13)$$

where  $M$  is the property of the material and  $C$  is the material distribution of the compounds in vector form.  $X$  and  $Y$  are determined as weights, and  $X$  and  $Y$  weights are regulated by the training process to suit every physical property. Since composite gratings are of  $8 \times 8$  and  $16 \times 16$  sizes, they standardize for every model for all 3 properties of fiber material. The determination of the resulting coefficient ( $D^2$ ) for the adjusted line is 0.916. Then, the mean absolute error ratio represents the limitations and

generalization issues by the linear model; then, the modulus exceeds the mean absolute error percentage (25%), and the toughness and strength are as high as 200% and 40%. As  $16 \times 16$  grid size, the outcomes of the linear model are determination coefficient ( $D^2$ ) of 0.928; then, the values of MAPE are maximum with 21%, 32%, and 127% for modulus, strength, and toughness. High error standards are generated from the linear model to explain the CNN for the prediction problem. Figure 9 and 10 show that the ranked weights are determined by the dark color near to the tip crack, the light color is determined by the straight one at the crack tip as positive of soft fiber materials, and then colorless materials are determined by the negative as stiff fiber materials. These composite mechanical properties have high accuracy.

The CNN is used in signal processing and recognition of images and is also utilized to extract geographies from datasets. Before the inference process, CNN models must be developed. The training process is a problem of optimization; then, the MSE is minimized by the optimal collection of the weight of the model CNN. To begin the training process, it required many examples of dataset; then, the input and output data determine the approximate relationship by optimal mapping. Then, the CNN model uses 200 training periods; it is an iteration of the CNN model training process. A single epoch is concluded when on each training the CNN model is trained with examples in the dataset. The 200 epochs are used meeting the CNN model on each example of training of about 200 times of the set of training data. Figures 11 and 12 show the loss functions of test convergence history and drive for  $8 \times 8$  and  $16 \times 16$  grids. The loss function of MSE of all mechanical properties for two sizes of the grid converges with very low standards. The variance between test and training sufferers after the 200 epochs is small and there is no serious overflow occurring. The CNN model developed and produced the best problematic results and predicted the three properties of fiber materials with great precision.

After the process of training, estimate the CNN model performance using the 3 parameters, the mean absolute error ratio, data points percentage, and maximum error with an error maximum of 5%. These parameters are measured by testing the data set that is nongenerated by the CNN during the process of model creation. The performance of the CNN model is illustrated in Tables 2 and 3. Resistance, toughness, and MAPE modulus are less than 5%. A stronger limit for estimating the activity of the CNN is the extreme error. The extreme strength and error in the module are greater than 5%. But the data points' number larger than 5% error is meager,  $8 \times 8$  grid has 1.7%, and  $16 \times 16$  has 0.082%.

**4.1. Shielding Performance.** The EMI samples results A2, A3, A2H11, and A3H12 in a range of 10 GHz are compared and examined as given in Figure 13. The EMI shielding was intensely improved after the A1 sheets are presented because of the good shielding property. The EMI samples A2, A3, A2H11, and A3H12 are 1.0–4.8 dB, 1.4–6.3 dB, 30.7–46.8 dB, and 28.5–53.5 dB as in

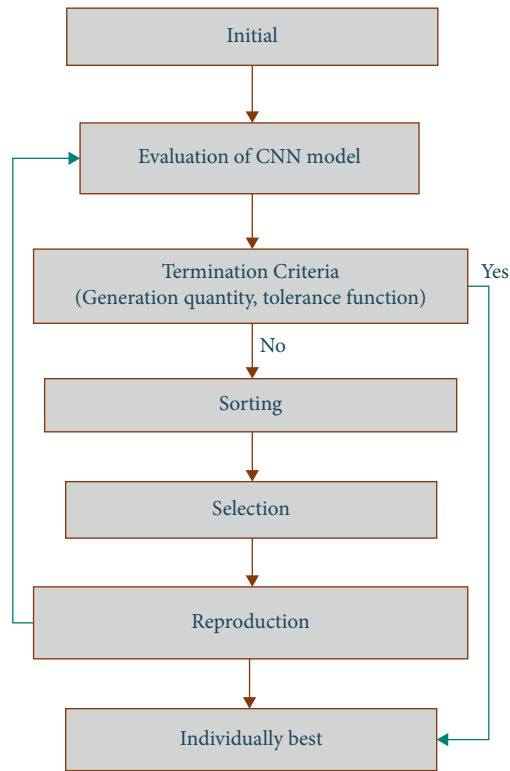


FIGURE 8: Flowchart of genetic algorithm process.

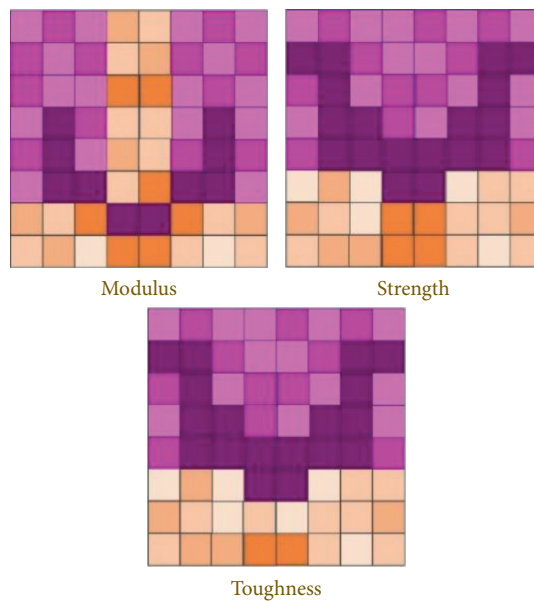


FIGURE 9: 8 × 8 grid weights ranking.

Figure 13(a). Comparing the control samples, EMI shielding improves the samples A2H11, and A3H12 are important. The samples EMI shielding performance A2H11 and A3H12 are on the needed values of EMI shielding in applications. Figure 13(b) represents the reflection in EMI of A2, A3, A2H11, and A3H12 composites which were 10.1–17.3%, 17.0–29.8%, 52.6–79.4%, 56.0–80.6%. The EMI shielding values from the absorption

and multiple-reflection of the composites were 82.7%–89.9%, 70.2%–83.0%, 20.6–47.4%, and 19.4–44.0%, Figure 13(c). The natural fiber composites have low EMI, while the composites with A1 sheets presented much more reflection. The EMI reflections of A2H11 and A1H12 minimized the A1 sheet measured as 83.7–93.9%. During the reflection and incidence, materials absorb EMI waves; it will reduce the shielding efficiency.

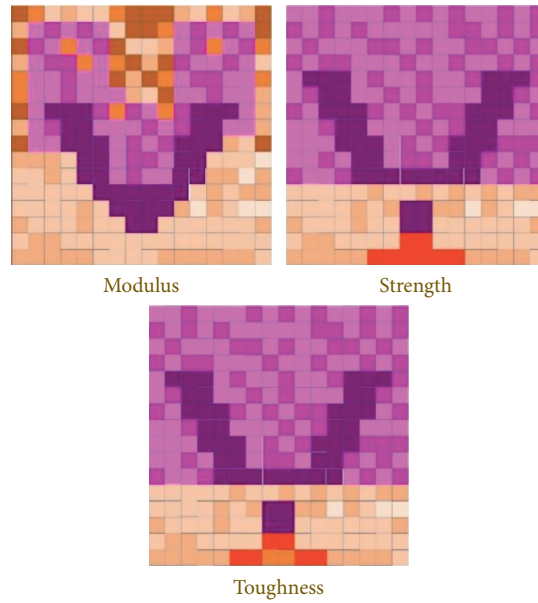


FIGURE 10: 16 × 16 weights ranking.



FIGURE 11: The convergence loss function history of the 8 × 8 grid.

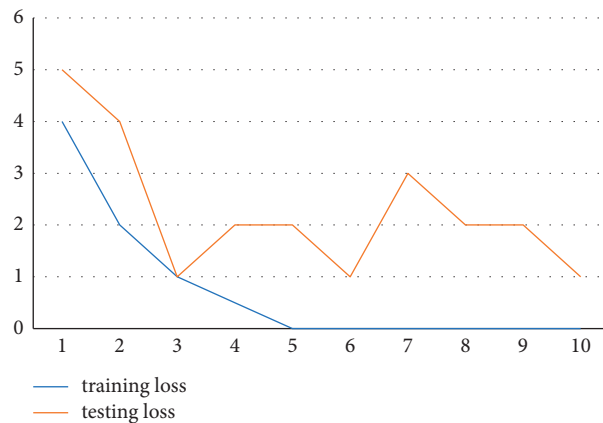


FIGURE 12: The convergence loss function history of the 16 × 16 grid.

4.2. GA Optimizer. The genetic algorithm optimization method is applied to optimize the maximal tensile strength function with GA. The strains receive the output value of the

best tensile strength, the bending strength. The maximum impact force and results were gained during the repetition in the GA method.

TABLE 2: CNN model performance for 8 × 8 grid.

|           | MAPE (%) | Max error (%) | Data points with error % > 5 (%) |
|-----------|----------|---------------|----------------------------------|
| Modulus   | 0.6      | 0.7           | 0.0                              |
| Strength  | 0.2      | 0.4           | 0.0                              |
| Toughness | 0.8      | 38.8          | 1.7                              |

TABLE 3: CNN model performance for 16 × 16 grid.

|           | MAPE (%) | Max error (%) | Data points with error % > 5 (%) |
|-----------|----------|---------------|----------------------------------|
| Modulus   | 0.2      | 2.4           | 0.0                              |
| Strength  | 0.4      | 2.1           | 0.0                              |
| Toughness | 2.4      | 188.7         | 0.082                            |

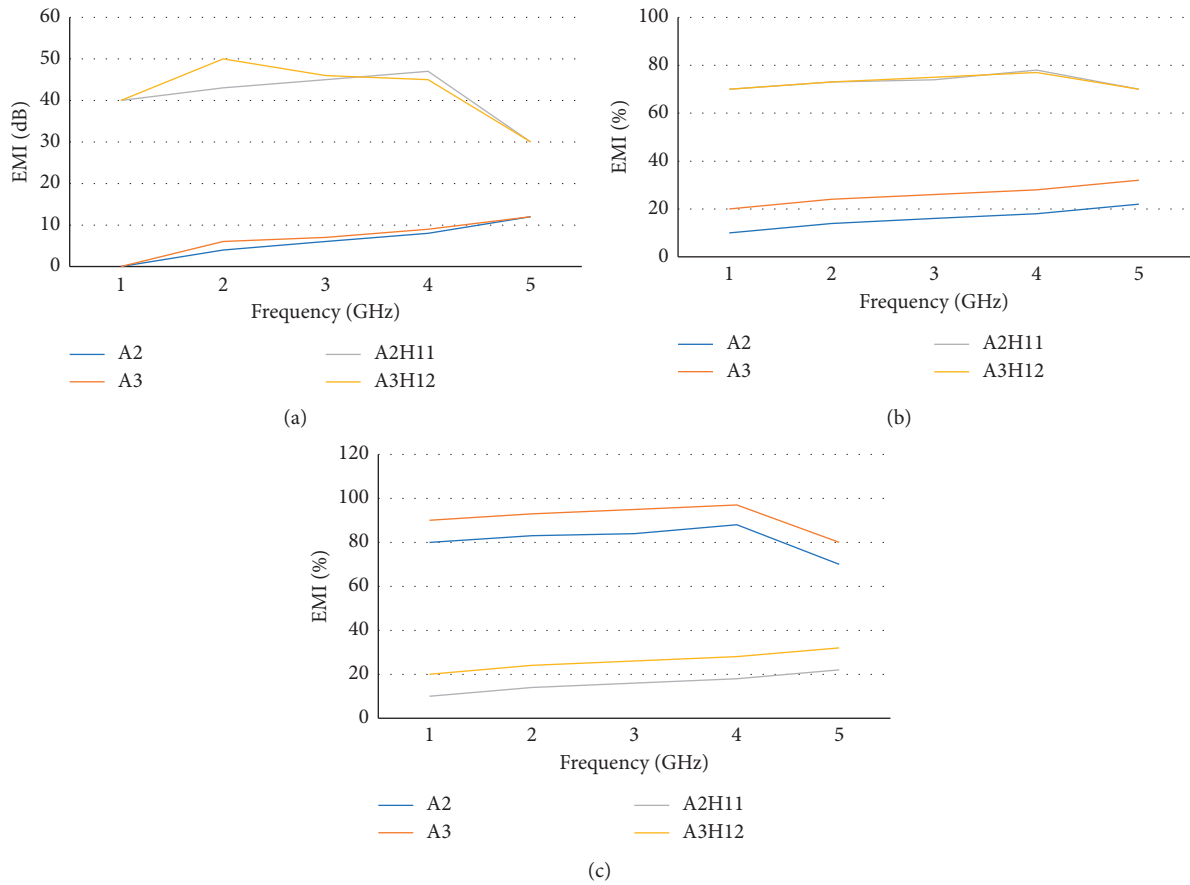


FIGURE 13: The shielding effectiveness of electromagnetic interference of the A2, A3, A3H11, and A2H12 composites. (a) Reflection contribution, (b) absorption, and (c) shielding efficiency.

Figure 14 shows the mathematical model and GA accuracy. The experimental and expected values were derived from the GA mathematical model:

$$\text{error (\%)} = 100 * \frac{(\text{expected} - \text{experimental})}{\text{predicted}}. \quad (14)$$

The combination of simultaneous optimization has four possibilities: (a) the strength and the module, (b) the toughness and the module, (c) the toughness and the strength, and (d) the toughness of the module and the strength. The objective aggregate function (AOF), which combines the various objects into the scalar function,

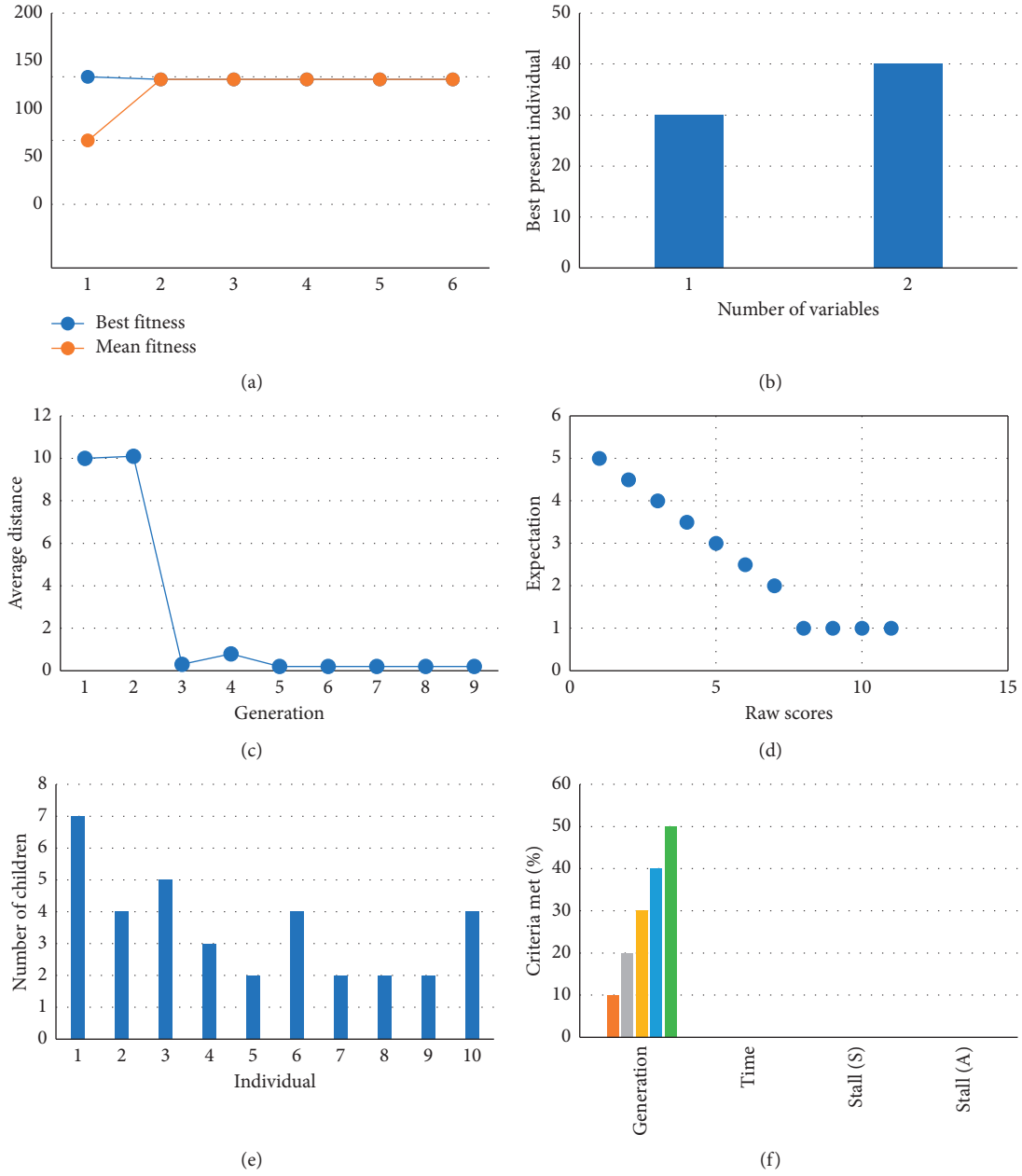


FIGURE 14: GA optimization method. (a) Best and mean fitness. (b) Present best individual. (c) Average distance between individuals. (d) Scaling fitness. (e) Selection function. (f) Stopping criteria.

depends on the simple biased objective amount that works poorly in the nonconvex case. One solution is used for programming compromise:

$$\text{AOF} = E_m t_m^x + E_s t_s^x + E_t t_t^x, \quad (15)$$

$$\begin{aligned} T_m &= \frac{\text{modulus}}{\text{maximum modulus}}, \\ T_s &= \frac{\text{strength}}{\text{maximum strength}}, \\ T_t &= \frac{\text{toughness}}{\text{maximum toughness}}, \end{aligned} \quad (16)$$

where  $x$  is the objective exponent function, and it is selected to be  $x=4$ . Then  $E_m$ ,  $E_s$ , and  $E_t$  are the masses of modulus, strength, and toughness. When optimizing two properties, the weight matching to the properties and then optimized for the assigned value is 0.5. Then the third property of the attributed weight value is 0.0. For three properties, the value of each of the three weightings is 0.333. In addition, the various goals have various scales which can cause bias to higher values of the goals. This issue is determined by each normalizing target by its maximum value as shown in (16).

Figure 15 and Table 4 show the outcome result derived from the optimizer GA when the multiobjective is measured with the checkerboard material. From the optimization of

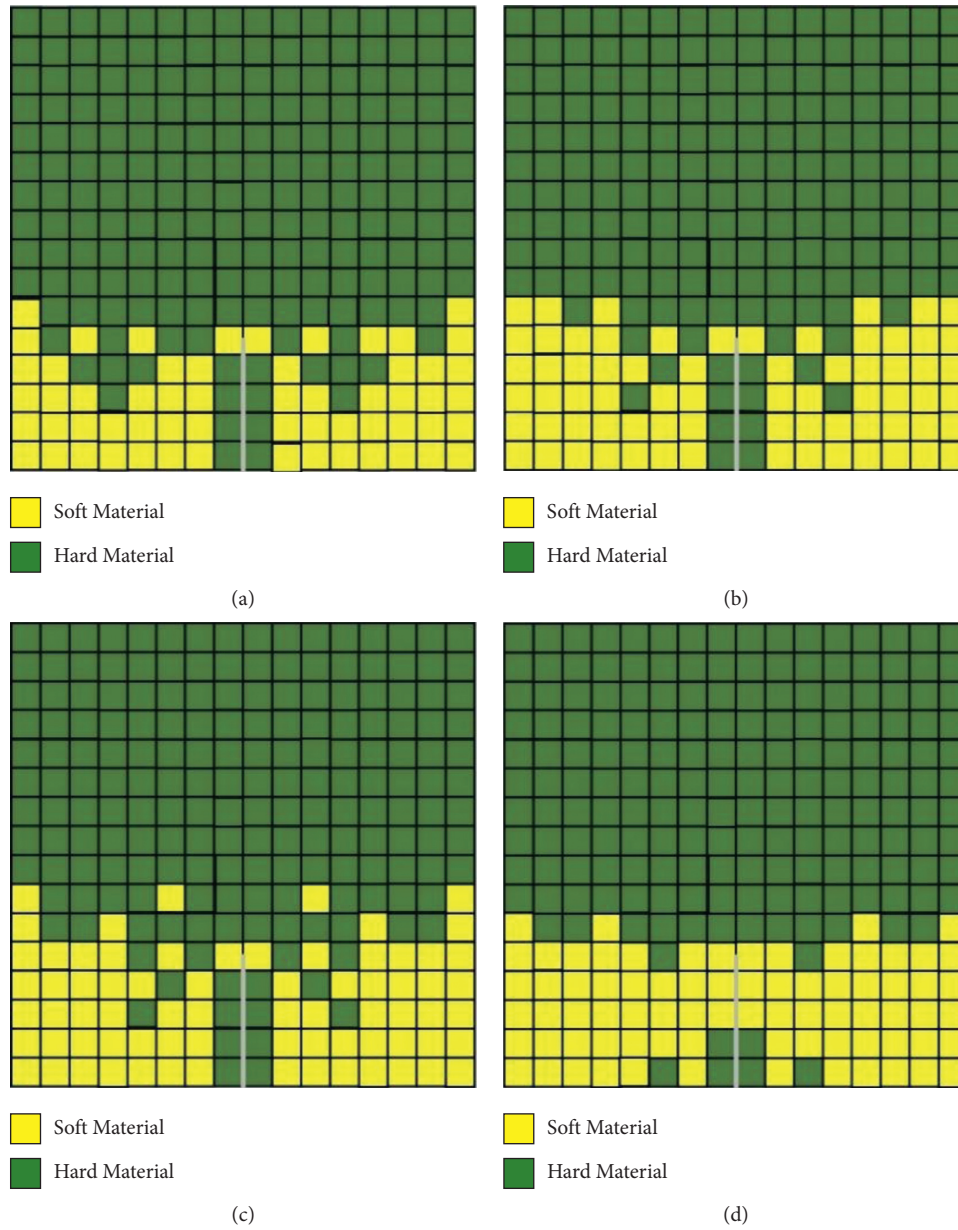


FIGURE 15: Optimization of multiobjective using GA method.

TABLE 4: Results of optimization using GA.

| Output                                     | Strength and modulus | Toughness and modulus | Toughness and strength | Modulus, strength, and toughness |
|--|----------------------|-----------------------|------------------------|----------------------------------|
| The fractional volume of soft material (%) | 23.4                 | 27.3                  | 28.1                   | 32.8                             |
| $T_s$                                      | 0.99                 | 0.99                  | 0.99                   | 0.97                             |
| $T_m$                                      | 0.84                 | 0.81                  | 0.79                   | 0.76                             |
| $T_t$                                      | 0.86                 | 0.94                  | 0.94                   | 0.97                             |

single-objective, the material is not soft, so the modulus is maximum. But when optimizing toughness or strength in addition to the module, the optimizer allows for equilibrium of the various purposes. The modulus determined from optimization of multiobjective is importantly minimized

due to the soft materials, and the soft fiber material volume segment ranges from 23% to 33% depending on the materials that are optimized. Then, the configuration of strength high values and the toughness of fiber materials have a good synchronization. The optimizer inclines to

bundle the flexible fiber material at the location next to the tip of the crack. Therefore, less compromise is required.

## 5. Conclusion

An approach to analyze the mechanical properties of natural fiber composites for modeling and optimization methods was developed, such as RoHM, CNN, and GA methods to improve properties and usage. The techniques for application modeling in NFC allowing to identify and isolate the various parameters that have an important effect on the outcoming materials are carried out to the optimization. The convolution neural network (CNN) is established to predict the mechanical properties of NFC composites by considering the checkboard of two sizes of  $8 \times 8$  and  $16 \times 16$  grid. The grid model is used to determine the module, strength, and tenacity of the material. It has shown the potential for using CNN in hardware and structural study. The composites represent the shielding performance of EMI with better mechanical properties as the structure of EMI shielding materials. The development of the model CNN is combined with a GA optimizer to find the fraction of volume of the composite material configuration to enhance performance. The optimization of GA results from the mechanical property of fiber length and content. There is better agreement between values of experimental and predicted values. CNN models take the accelerating potential of present optimization methods, and they develop the field of material and structural design.

## Data Availability

The data used to support the findings of this study are included within the article.

## Conflicts of Interest

The authors declare that there are no conflicts of interest regarding the publication of this article.

## Acknowledgments

The authors would like to express their gratitude towards Saveetha School of Engineering, Saveetha Institute of Medical and Technical Sciences (formerly known as Saveetha University), for providing the necessary infrastructure to carry out this work successfully.

## References

- [1] R. Anandkumar, S. Ramesh Babu, and R. Sathyamurthy, "Investigations on the mechanical properties of natural fiber granulated composite using hybrid additive manufacturing: a novel approach," *Advances in Materials Science and Engineering*, vol. 2021, pp. 1–12, 2021.
- [2] S. Velumani, P. Navaneetha Krishnan, and S. Jayabal, "Mathematical modeling and optimization of mechanical properties of short coir fiber-reinforced vinyl ester composite using genetic algorithm method," *Mechanics of Advanced Materials and Structures*, vol. 21, no. 7, pp. 559–565, 2014.
- [3] S. Ferdous and S. Hossain, "Natural fibre composite (NFC): new gateway for jute, kenaf and allied fibres in automobiles and infrastructure sector," *World J Res Rev*, vol. 5, no. 3, pp. 35–42, 2017.
- [4] K. Salasinska and J. Ryszkowska, "The effect of filler chemical constitution and morphological properties on the mechanical properties of natural fiber composites," *Composite Interfaces*, vol. 22, no. 1, pp. 39–50, 2015.
- [5] M. Alhijazi, Q. Zeeshan, Z. Qin, B. Safaei, and M. Asmael, "Finite element analysis of natural fibers composites: a review," *Nanotechnology Reviews*, vol. 9, no. 1, pp. 853–875, 2020.
- [6] S. Mahesh and D. G. Ramkumar, "Smart face detection and recognition in low resolution images using alexnet CNN compare accuracy with SVM," *Alinteri Journal of Agriculture Sciences*, vol. 36, no. 1, pp. 721–726, 2021.
- [7] G. Ramkumar, G. Anitha, S. Suresh kumar, M. Ayyadurai, and C. SenthilKumar, "An effectual underwater image enhancement using deep learning algorithm," in *Proceedings of 2021 5th International Conference on Intelligent Computing and Control Systems (ICICCS)*, vol. 2021, 2021.
- [8] Dr Govindaraj, "Face recognition based on spatio angular using visual geometric group- 19 convolutional neural network," *Annals of the Romanian Society for Cell Biology*, vol. 25, pp. 2131–2138, 2021.
- [9] Y. S. Munde and R. B. Ingle, "Theoretical modeling and experimental verification of mechanical properties of natural fiber reinforced thermoplastics," *Procedia Technology*, vol. 19, pp. 320–326, 2015.
- [10] R. de Araujo Alves Lima, D. Kawasaki Cavalcanti, J. de Souza e Silva Neto et al., "Effect of Surface Treatments on Interfacial Properties of Natural Intralaminar Hybrid Composites," *Polymer Composites*, vol. 41, no. 1, pp. 314–325, 2020.
- [11] V. Sridharan and N. Muthukrishnan, "Optimization of machinability of polyester/modified jute fabric composite using Grey relational analysis (GRA)," *Procedia Engineering*, vol. 64, pp. 1003–1012, 2013.
- [12] N. Sultana, S. M. Zakir Hossain, and M. S. Alam, M. S. Islam, M. S. Islam, and M. A. A. Abtah, "Soft computing approaches for comparative prediction of the mechanical properties of jute fiber reinforced concrete," *Advances in Engineering Software*, vol. 149, no. November, Article ID 102887, 2020.
- [13] Z. L. Wang, J. Wu, and J. G. Wang, "Experimental and numerical analysis on effect of fibre aspect ratio on mechanical properties of SRFC," *Construction and Building Materials*, vol. 24, no. 4, pp. 559–565, 2010.
- [14] M. S. Islam, N. A. B. Hasbullah, M. Hasan, Z. A. Talib, M. Jawaid, and M. K. M. Haafiz, "Physical, mechanical and biodegradable properties of kenaf/coir hybrid fiber reinforced polymer nanocomposites," *Materials Today Communications*, vol. 4, pp. 69–76, 2015.
- [15] L. Kerni, S. Singh, A. Patnaik, and N. Kumar, "A review on natural fiber reinforced composites," *Materials Today: Proceedings*, vol. 28, pp. 1616–1621, 2020.
- [16] K. L. Pickering, M. G. A. Efendy, and T. M. Le, "A review of recent developments in natural fibre composites and their mechanical performance," *Composites Part A: Applied Science and Manufacturing*, vol. 83, pp. 98–112, 2016.
- [17] D. K. K. Cavalcanti, M. D. Banea, J. S. S. Neto, R. A. A. Lima, L. F. M. Da Silva, and R. J. C. Carbas, "Mechanical characterization of intralaminar natural fibre-reinforced hybrid composites," *Composites Part B: Engineering*, vol. 175, Article ID 107149, 2019.

- [18] A. Subasinghe, R. Das, and D. Bhattacharyya, "Study of thermal, flammability and mechanical properties of intumescent flame retardant PP/kenaf nanocomposites," *International Journal of Social Network Mining*, vol. 7, no. 3, pp. 202–220, 2016.
- [19] A. Pappu, K. L. Pickering, and V. K. Thakur, "Manufacturing and characterization of sustainable hybrid composites using sisal and hemp fibres as reinforcement of poly (lactic acid) via injection moulding," *Industrial Crops and Products*, vol. 137, pp. 260–269, 2019.
- [20] M. Boopalan, M. Niranjanaa, and M. J. Umaphathy, "Study on the mechanical properties and thermal properties of jute and banana fiber reinforced epoxy hybrid composites," *Composites Part B: Engineering*, vol. 51, pp. 54–57, 2013.
- [21] K. P. Ashik and R. S. Sharma, "A review on mechanical properties of natural fiber reinforced hybrid polymer composites," *Journal of Minerals and Materials Characterization and Engineering*, no. 5, pp. 420–426, 2015.
- [22] N. Venkateshwaran, A. Elayaperumal, and G. K. Sathiya, "Prediction of tensile properties of hybrid-natural fiber composites," *Composites Part B: Engineering*, vol. 43, no. 2, pp. 793–796, 2012.
- [23] G. Arani, H. B. Ali, Z. Akbar, and E. Haghparast, "Application of halpin-tsai method in modelling and size-dependent vibration analysis of CNTs/fiber/polymer composite microplates," *Journal of Computational and Applied Mechanics*, vol. 47, no. 1, pp. 45–52, 2016.
- [24] S. S. Shinde, A. V. Salve, and S. Kulkarni, "Theoretical modeling of mechanical properties of woven jute fiber reinforced polyurethane composites," *Materials Today: Proceedings*, vol. 4, no. 2, pp. 1683–1690, 2017.
- [25] G. Ramkumar, R. Thandaiah Prabu, N. Phalguni Singh, and U. Maheswaran, "Experimental analysis of brain tumor detection system using Machine learning approach," *Materials Today: Proceedings*, 2021, In press.
- [26] Y.-W. Jung and H.-K. Kim, "Prediction of nonlinear stiffness of automotive bushings by artificial neural network models trained by data from finite element analysis," *International Journal of Automotive Technology*, vol. 21, no. 6, pp. 1539–1551, 2020.
- [27] S. Ye, B. Li, Q. Li, H.-P. Zhao, and X.-Q. Feng, "Deep neural network method for predicting the mechanical properties of composites," *Applied Physics Letters*, vol. 115, no. 16, Article ID 161901, 2019.
- [28] G. Ramkumar and E. Logashanmugam, "Hybrid framework for detection of human face based on haar-like feature," *International Journal of Engineering & Technology*, vol. 7, no. 3, pp. 1786–1790, 2018.
- [29] A. Jaramillo-Botero, S. Naserifar, and W. A. Goddard III, "General multiobjective force field optimization framework, with application to reactive force fields for silicon carbide," *Journal of Chemical Theory and Computation*, vol. 10, no. 4, pp. 1426–1439, 2014.